JOURNAL OF MATERIALS SCIENCE 28 (1993) 5387–5396

The Williams–Watts dependence as a common phenomenological approach to relaxation processes in condensed matter

F. L. CUMBRERA, F. SANCHEZ-BAJO, F.GUIBERTEAU, J. D. SOLIER
Department of Physics, Faculty of Science, University of Extremadura, Badajoz, Spain
A. MUÑOZ
Department of Physics of Condensed Materials, Faculty of Science, University of Seville, Seville, Spain

The Williams–Watts (WW) relaxation function has been widely used to describe the relaxation behaviour of many systems. In the present work the range of applicability of the WW response was extensively tested by the analysis of experiments in both the time and the frequency domains. On the other hand, the analysed experiments covered a wide time-scale for the characteristic relaxation times. Some related topics were also considered, i.e. our procedures in obtaining the associated activation energy spectra or the distribution of relaxation times. The relationship between time–domain and frequency–domain relaxation responses was also analysed. In light of our results the universality of the WW response, appears to be good at least for the time-scales and the different probes covered by our experiments.

1. Introduction

The relaxation phenomena include all the processes establishing equilibrium in a system which is in a non-equilibrium state. They may be observed on a wide variety of phenomena and materials. Among the relaxation processes, we selected for consideration the most representative of them, namely mechanical, structural and dielectric relaxation.

Analysis of relaxation results has often used empirical response functions [1, 2]. In particular, the empirical function proposed by Williams and Watts (WW) [3] for the fitting of dielectric loss and dispersion, provides an excellent description for the analysis of many glassy materials in the vicinity of the glass transition temperature, T_g [4–6]. The relaxation of spin-glasses near the freezing temperature is also well described by the WW law [7, 8]. In the spin-glasses, their empirical WW relaxation function is frequently termed the stretched exponential function. Montroll and Bendler [9] and MacDonald [10] have emphasized how the Lévy-stable distribution of relaxation times leads to the WW response. The latter author claimed only limited applicability of the WW function: the Lévy distribution has no finite moments and it is inconsistent with processes occurring in a material of finite size.

In the present work we considered the application of the WW relaxation function to the analysis of the following phenomena:

(a) mechanical stress relaxation in compression tests on CoO single crystals betwen 77 and 289 K;

(b) enthalpic relaxation in amorphous selenium around T_g, and

(c) dielectric relaxation of Y_2O_3-fully stabilized ZrO_2 (Y-FSZ, 9.4% mol yttria).

It is noteworthy that this set of diverse experiments covers the broad interval between 10^{-5} and 10^{7} s for the characteristic relaxation times. We begin by presenting the experimental results of the above mentioned relexation phenomena. Next, we discuss and compare these results in terms of the WW law. Then, we include our procedure in obtaining the distribution function of relaxation times (DRT), $g(\tau)$, where τ is the relaxation time associated with an elemental process. Some comments about the method of successive approximations of Agrawal and Zhang [11] are added. Because the equations governing the response of relaxing systems may be described by either a DRT function or an activation energy spectrum (AES), we establish the AES associated with the WW behaviour. A sophisticated method, which improves the Primak "energy derivative" approximation [12], is used to calculate the detailed shape of the spectrum. Finally, in light of the above results, we support the usefulness of the WW description in the frame of linear relaxation phenomena.

2. Experimental procedure

2.1. Mechanical relaxation experiments

In order to test the validity of the WW law for this kind of experiment we employed CoO single crystals

0022–2461

which were grown by the zone-melted technique in an arc image furnace. The sintered rod which feeds the melt was obtained from high-purity powder (Johnson Mattey). The crystals were oriented using the back-reflection Laue X-ray technique; they were cut along (1 0 0) faces to give parallelepipeds of sizes between $2 \times 2 \times 5$ mm^3 and $3 \times 3 \times 5$ mm^3. The specimens were annealed in air to 1473 K for 2 days and air-quenched to room temperature prior to mechanical testing.

Compression tests at a constant crosshead velocity (20 μm min^{-1}, strain rate $\dot{\varepsilon} = 7 \times 10^{-5}$ s^{-1}) were performed in an Instron machine with the equipment already described [13, 14]. The temperatures selected were 77, 273 and 293 K (room temperature). In this temperature interval, the yield stress, $\sigma_{0.2\%}$, increases very quickly as temperature decreases below 273 K [14] suggesting a thermally activated mechanism which controls the glide of dislocations. For each temperature, relaxation stress tests were achieved at two different plastic strains (0.5% and 1%). In the relexation experiments the crosshead is abruptly stopped in the plastic domain at the initial external stress, $\sigma(0)$, and, subsequently, the system progresses towards its new equilibrium condition so that the instantaneous external stress, $\sigma(t)$, decreases with time towards its final value, $\sigma(\infty)$.

2.2. Enthalpic relaxation experiments through the T_g region

The experiments of enthalpic relaxation analysed in the present work, which were conducted using a Perkin–Elmer DSC-IIC differential scanning calorimeter, were described in detail elsewhere [15, 16]. In order to achieve the best repetitivity of the measurements, the rejuvenation method or cyclic experiment (cooling–annealing–heating) was adopted [16–18]. Such an experiment consists in cooling the sample through the T_g zone, from T_0 (in an equilibrium state) to T_v (temperature of isothermal hold), and subsequent reheating to T_0. The cooling and heating rates were similar (Table 1 summarizes the main parameters defining the experimental conditions).

The following substantial advantages may be expected from the cyclic experiment schedule.

(i) All experiments are carried out on the same amorphous sample. In practice, this question is very important because small changes in the preparation conditions can often produce large changes in the relaxation rates of the glass.

(ii) The experiment may be modified to allow a more complicated T-history (e.g. two or more T-steps) for which it is much easier to separate the thermal and structural contributions to the elemental relaxation times.

TABLE I. Values of the parameters defining the DSC cyclic experiment. Cp_l, Cp_g and ΔCp are, respectively, the measured values for the heat capacity of the liquid and the glass and its difference

T_0	340 K
T_v	296 K
$q^+ = \lvert q^- \rvert$	20 K min^{-1}
Cp_l	35.68 J mol^{-1} K^{-1}
Cp_g	24.42 J mol^{-1} K^{-1}
ΔCp	11.26 J mol^{-1} K^{-1}

With respect to the amorphous selenium samples, thin films about 1.5 μm thick were prepared by the vacuum evaporation of Johnson-Mattey selenium (99.999% purity) at the residual pressure of 2×10^{-4} Pa. Glass substrates were used and kept at room temperature during deposition. The non-crystallinity of the specimens was checked on control samples by means of calorimetric scan tests and transmission electron microscopy (TEM) experiments including selected-area electron diffraction (SAD).

2.3. Dielectric relaxation experiments

Samples for this study were single crystals of 9.4 mol% Y_2O_3-fully stabilized ZrO_2 (Y-FSZ) grown by the Skull melting method. These samples were oriented by the Laue X-ray back-reflection technique such that crystals with 10 mm × 10 mm major surfaces parallel to {1 0 0} or {1 1 1}, about 450 μm thick, were cut, polished and finished with 3 μm diamond paste. Gold electrodes were then evaporated on both major faces.

Measurements were performed by the two-probe complex impedance dispersion technique in the range between 423 and 673 K. Temperature was controlled to ± 1 K for this kind of experiment. The frequencies analysed were between 100 Hz and 1 MHz.

3. The Williams–Watts response function

The course of relaxation is controlled by the change of a certain parameter, $P(t)$, which is connected with the degree of deviation of the system from equilibrium. For the normalization of the response, the following function of $P(t)$ is convenient

$$\phi(t) = \frac{P(t) - P(\infty)}{P(0) - P(\infty)} \tag{1}$$

t being the time, and where we denote in brackets the appropriate instances of time. The most widely used function which represents $\phi(t)$ was proposed by Williams and Watts [3]

$$\phi(t) = \exp[-(t/\tau_0)^{\beta}] \tag{2}$$

τ_0 being a characteristic relaxation time and β ($0 < \beta \leq 1$) is a non-dimensional relaxation parameter which is inversely proportional to the relaxation-time–distribution width.

It is postulated [9] that $\phi(t)$ might be expressed as a superposition of single relaxation exponentials

$$\phi(t) = \int_0^{\infty} g(\tau) e^{-t/\tau} d\tau \tag{3}$$

where $g(\tau)$ is a normalized distribution of relaxation times

$$\int_0^{\infty} g(t)\, d\tau = 1 \tag{4}$$

The average relaxation time may be written as

$$\langle\tau\rangle = \frac{\tau_0}{\beta}\Gamma(1/\beta) \tag{5}$$

corresponding to the integrated area of the WW function. Higher moments are given by

$$\langle\tau^n\rangle = \int_0^\infty \tau^n g(\tau)\,d\tau = \frac{\tau_0^n}{\beta}\frac{\Gamma(n/\beta)}{\Gamma(n)} \tag{6}$$

Likewise, average relaxation frequencies can be defined

$$\langle\omega^n\rangle = \int_0^\infty \frac{1}{\tau^n} g(\tau)d\tau = (-1)^n \frac{d^n\phi(0)}{dt^n} \tag{7}$$

but the derivative of the WW function is given by

$$\frac{d\phi(t)}{dt} = -\frac{\beta}{\tau_0}(t/\tau_0)^{\beta-1}\phi(t) \tag{8}$$

which diverges at $t = 0$. Therefore, that the derivative diverges as $t \to 0$ could preclude a physical interpretation of the WW function [10, 19].

The formalism of the DRT has been shown to be of considerable value in understanding relaxation processes in amorphous materials. The way into derive the $g(\tau)$ function from the experimentally available τ_0 and β parameters will be considered later.

4. Results

4.1. Mechanical relaxation

We show in Fig. 1 the dependence of the relaxed stress

$$P(t) = \sigma(0) - \sigma(t) \tag{9}$$

with the elapsed time for a plastic strain of 0.5% and the three selected temperatures mentioned above.

In a qualitative fashion we observe the following outstanding features:

(i) the time to reach the final equilibrium increases with increasing the temperature;

(ii) likewise, the asymptotic $P(\infty)$ value, which indicates the whole relaxed stress, increases with increasing T;

(iii) the shape of the curve relative to 77 K is clearly different to those representative of 273 and 289 K.

Taking into account our definition of $P(t)$ for this kind of experiment, we have $P(0) = 0$. Thus one can write

$$P(t) = P(\infty)[1 - e^{-(t/\tau_0)^\beta}] \tag{10}$$

We now attempt to calculate the characteristic parameters of the WW law: τ_0 and β. A note should be added here concerning the difficulty of obtaining accurate values of $P(\infty)$ except for the lowest temperature experiment. Therefore, we have, in fact, three adjustable parameters in Equation 10 (namely, τ_0, β and $P(\infty)$) which can be obtained by using a non-linear least-squares routine. In practice, we have applied the Levenberg–Marquardt method [20] and the results are reported in Table II. A quick look at these results confirms the qualitative observations already mentioned. Moreover, the shape of the curves, which depends on the β exponent, proved to be similar (within experimental error) for the highest temperature experiments but different from that obtained at 77 K. By using the non-dimensional coordinates $P(t)/P(\infty)$ and t/τ_0 we show in Fig. 2 the coincidence of the curves corresponding to the higher temperatures. A similar consideration may be done from Fig. 3 where the same non-dimensional representation is performed for 77 K and the two plastic strains analysed. From Fig. 3 and Table II it is clear that the only meaningful change observed when increasing the plastic strain corresponds to a small increase in the asymptotic value $P(\infty)$.

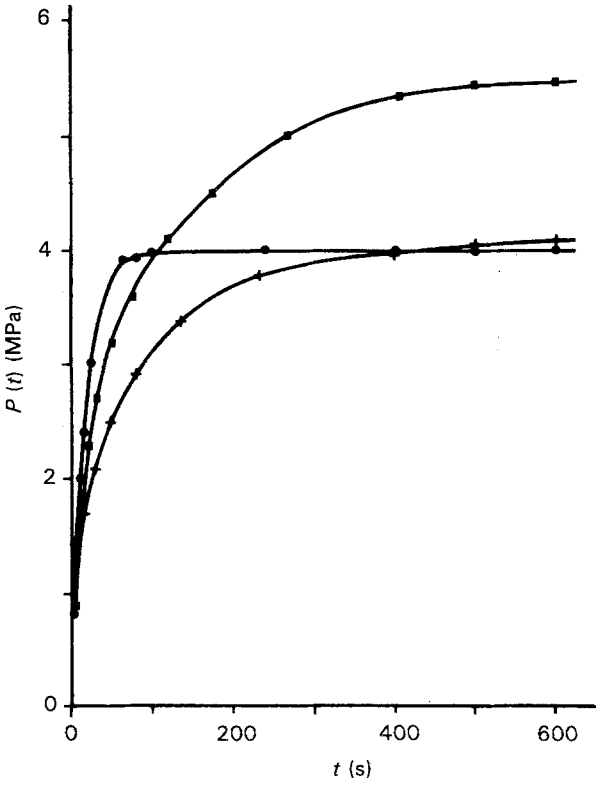

Figure 1 Time dependence of the relaxed stress for the CoO samples at a 0.5% plastic strain and the experimental temperatures: (●) 77 K, (+) 273 K and (■) 289 K).

TABLE II Levenberg–Marquardt least-squares fit parameters of the WW dependence for mechanical relaxation experiments

T (K)	ε(%)	$P(\infty)$ (MPa)	τ_0 (s)	β
77	0.5	4.0 (1)[a]	14.7 (4)	0.83 (2)
	1	4.3 (1)	16.3 (4)	0.81 (2)
273	0.5	4.2 (2)	54 (2)	0.57 (3)
	1	4.6 (2)	41 (2)	0.66 (3)
289	0.5	5.69 (3)	71 (4)	0.55 (3)
	1	7.28 (5)	73 (5)	0.62 (4)

[a] The figures in parentheses, here and elsewhere in the tables, indicate the standard deviations (referred to the least significant digit) as estimated in the refinement.

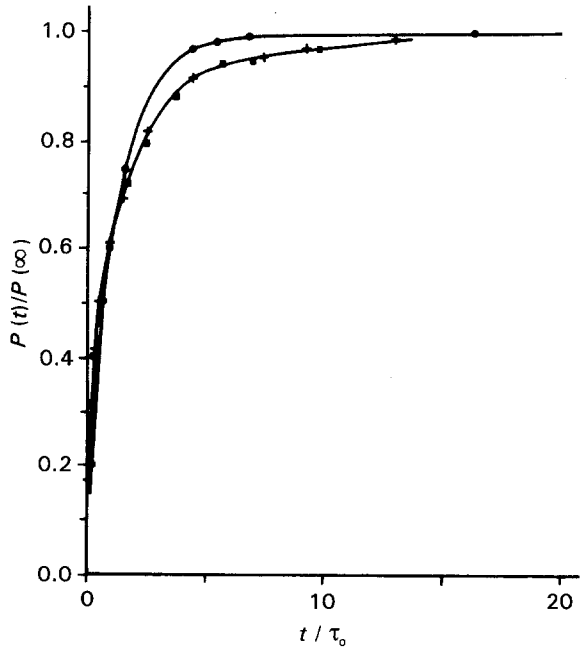

Figure 2 Comparison of the mechaical relaxation responses in a non-dimensional plot. The coincidence of the curves for the higher temepratures may be observed. (●) 77 K, (+) 273 K, (■) 289 K.

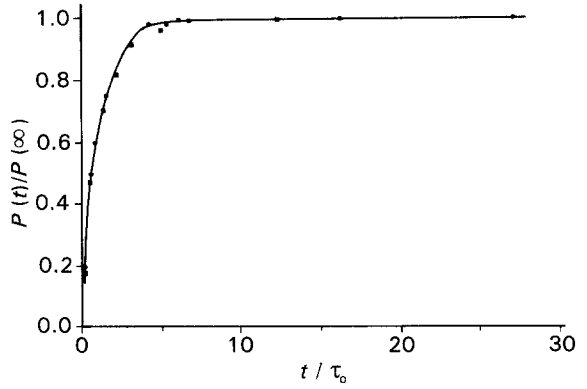

Figure 3 Non-dimensional plot as in Fig. 2, but for 77 K and the two plastic strains analysed: (●) 142 MPa, (■) 158 MPa.

Several theoretical approaches have been proposed to interpret the stress relaxation experiments [21–25]. The equation describing the plastic strain rate during the relaxation, $\dot{\varepsilon}_p$, is given by

$$\dot{\varepsilon}_p = -\dot{\varepsilon}_1 = -\frac{\dot{\sigma}}{E_c} \tag{11}$$

where E_c is the combined elastic modulus of the specimen–machine system and $\dot{\varepsilon}_1$ is the elastic strain rate. Thus, during the test the sample continues to deform plastically at a decreasing rate under the action of a decreasing applied stress. On the other hand, if the mobile dislocation density, ρ_m, is unchanged during the test, the $\dot{\varepsilon}_p$ dependence express the evolution of the dislocation velocity according to the Orowan equation

$$\dot{\varepsilon}_p = \gamma \rho_m \boldsymbol{b} \bar{v} \tag{12}$$

where γ is a geometric factor, $\boldsymbol{b}$ the length of the Burgers vector and $\bar{v}$ the average dislocation velocity. In this case, the dislocation flow is related to the thermal activation of dislocations which is governed by a stress-dependent Gibbs free energy

$$\Delta G = \Delta G_0 - W \tag{13}$$

where W is the work done by the applied stress and ΔG_0 is the Gibbs free energy in the absence of any external constraint [26]. Then it may be interpreted that the applied stress decreases until the effective height of the barrier, $\Delta G_0 - W$, is sufficiently large to prevent the dislocations jumping over the barrier by thermal fluctuations. Thus the well-known reaction theory supports our qualitative observations (i) and (ii). In fact, tests performed at higher temperatures need more time and a greater relaxed stress, in order to stop the plastic deformation, than do the lower ones.

Finally, Fig. 4 shows how the relaxed stress $P(t)$ may be fitted to the empiric relationship of Feltham [27]

$$P(t) = \lambda \lg(1 + \upsilon t) \tag{14}$$

where υ is a constant and λ is associated with the activation volume [24], V^*, by

$$\lambda = \frac{kT}{V^* f} \tag{15}$$

f being the Schmid factor for the activated slip system ($f = 0.5$ in our case [14]). Such a relationship predicts that a plot of $P(t)$ versus $\lg t$ gives a straight line provided that $t \gg 1/\upsilon$. The magnitude of the activation volume and the temperature, stress and strain dependence assist in identifying the rate-controlling deformation mechanism [28]. The values obtained for the activation volume at 77 K ($\simeq 30\ \boldsymbol{b}^3$) and their strain independence, suggests that the Peierls mechanism is operative. This last result for the 77 K experiment is consistent with its calculated β value, fairly close to 1 (usual values for β are in the range 0.3–0.6) which

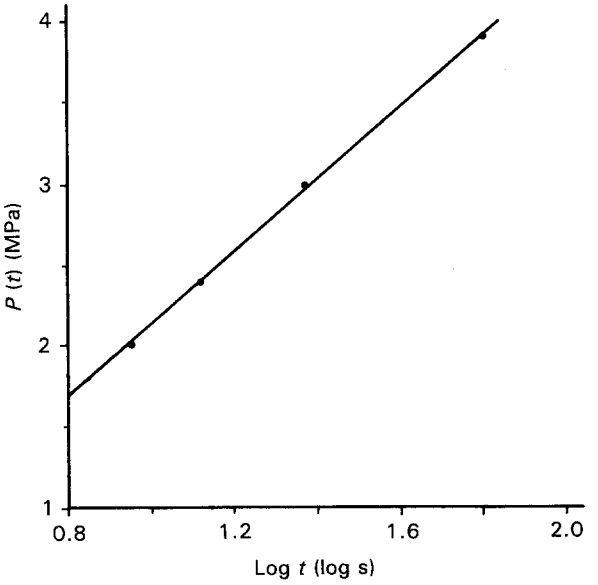

Figure 4 Feltham plot for the 77 K experiment.

supports the existence of a single mechanism controlling the low-temperature deformation.

4.2. Structural relaxation

Calorimetric measurements performed on amorphous selenium were the basis of this kind of experiment. Fig. 5 shows several DSC scans obtained after successive annealing stages at 296 K. During the cyclic experiments, all the heating or cooling rates were 20 K min^{-1}. Fig. 6 displays the experimental time dependence of $\phi(t)$ for several annealing temperatures lower than T_g when the excess enthalpy (the enthalpy relaxed during annealing and reabsorbed by the glass to reach its metastable equilibrium) was taken as the P property sensitive to the relaxation of amorphous selenium. In this figure, the solid lines correspond to the least-squares fit of the experimental data to the WW law allowing us to obtain the τ_0 and β values collected in Table III. As can be seen in the table an increase in the temperature of the isothermal hold decreases drastically the value of τ_0 and increases slightly the value of β. This last observation indicates

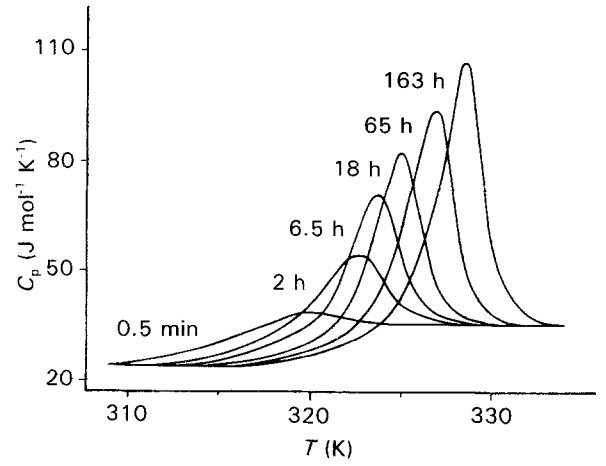

Figure 5 Heat capacity versus temperature through the glass transition region after successive annealing stages at 296 K. $q = 20$ K min^{-1}.

TABLE III Values of τ_0 and β obtained from the enthalpic relaxation of amorphous selenium at different temperatures

T (K)	τ_0 (h)	β
279	4874 (50)	0.36 (1)
296	16,3 (4)	0.41 (1)
305	3.0 (1)	0.43 (2)
309	0.89 (4)	0.52 (3)

a gradual narrowing of the associated DRT as we approach the glass transition temperature ($T_g \simeq 320$ K for a heating rate of 20 K min^{-1}).

4.3. Dielectric relaxation

The dielectric spectroscopy measures the response of materials to a sinusoidal electric field, E, of angular frequency, ω (usually in the range of audio or radio frequencies). The complex permittivity $\varepsilon^*(\omega)$ is the function relating the applied electric field and the resulting electric displacement, D. It is customary [4, 29] to introduce the complex dielectric modulus, $M^*(\omega)$, as the inverse of $\varepsilon^*(\omega)$. It has been shown [30] that

$$M^*(\omega) = 1/\varepsilon^*(\omega)$$
$$= M_s \int_0^\infty g(\tau)[i\omega\tau/(1 + i\omega\tau)]d\tau \quad (16)$$
$$= M_s \left\{1 - \int_0^\infty g(\tau)[1/(1 + i\omega\tau)]d\tau\right\}$$
$$= M_s[1 - N^*(\omega)] \quad (17)$$

where M_s is the high-frequency limit of the real part of $M^*(\omega)$, $g(\tau)$ corresponds to the above-mentioned normalized DRT and $N^*(\omega)$ is a relaxation function in the frequency domain. Moreover

$$N^*(\omega) = N'(\omega) - iN''(\omega)$$
$$= \int_0^\infty e^{-i\omega t}\left[-\frac{d\phi(t)}{dt}\right]dt \quad (18)$$

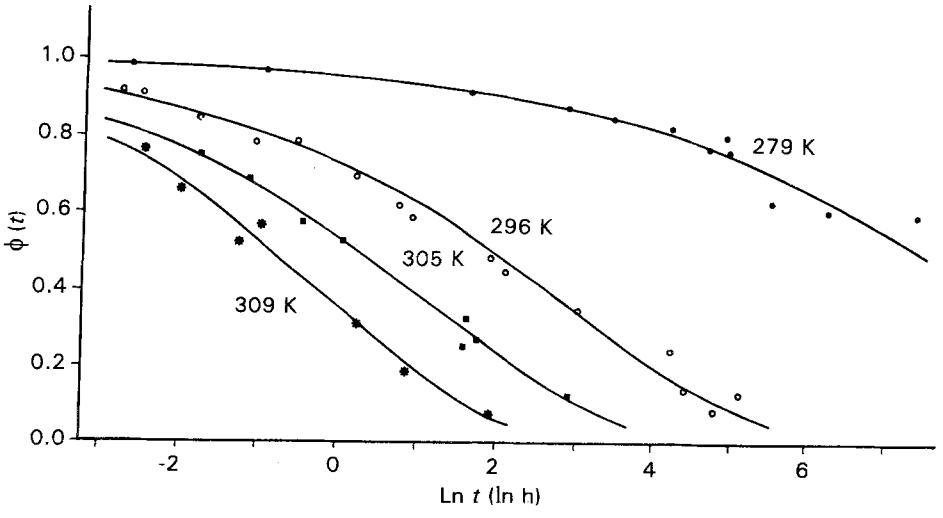

Figure 6 The excess enthalpy relaxation function corresponding to amorphous selenium for several annealing temperatures lower than T_g.

Thus, $N^*(\omega)$ may be expressed as the one-sided Fourier transform of the derivative of the relaxation function in the time domain.

Fig. 7 shows the real and imaginary parts of the complex dielectric modulus, $M'(\omega)$ and $M''(\omega)$, versus normalized frequencies for a Y-FSZ sample (the temperature of the experiment was 503 K). The shape of $M''(\omega)$, broad and skewed toward the high-frequency side, appears to call for a distribution of relaxation times.

In practice, the problem arises in relating the experimental response, $M^*(\omega)$, with the parameters τ_0 and β of the WW law describing the relaxation in the time domain. The most simple and rough way to derive these parameters for a sinusoidal excitation is to compare the experimental results with a set of previously calculated curves [4, 31]. Then, we try to fit the main characteristic features of the experimental curves: i.e. the maximum of $M''(\omega)$ and its position, the width of $M''(\omega)$ at half-height, the half-height position on the low frequency side, ..., etc. In the present paper we propose the following numerical approach: integration by parts yields

$$N^*(\omega) = 1 - i\omega\int_0^\infty e^{-i\omega t}\phi(t)dt \tag{19}$$

Then, if we let

$$\upsilon'(\omega) = \frac{N''(\omega)}{\omega} \tag{20}$$

$$\upsilon''(\omega) = \frac{1 - N'(\omega)}{\omega} \tag{21}$$

we find

$$\begin{aligned}\phi(t) &= \exp[-(t/\tau_0)^\beta] \\ &= 1/2\pi\left[\int_0^\infty \upsilon'(\omega)\cos\omega t\, d\omega\right. \\ &\quad \left. + \int_0^\infty \upsilon''(\omega)\sin\omega t\, d\omega\right]\end{aligned} \tag{22}$$

Subsequently, by using a linear fit of ln ln$[1/\phi(t)]$ versus ln t, it is easy to obtain the values of τ_0 and β which, in our case, were found to be $\tau_0 = 1.8 \times 10^{-5}$ s and $\beta = 0.57$.

Once we have derived the WW parameters, quite often the work is directed toward the determination of the associated $g(\tau)$ function [4, 9, 29]. In fact, $g(\tau)$ may be obtained from the inverse Laplace transformation of the WW decay function, as suggested by Pollard [32]. In many practical cases, a series expansion of the integral equation is performed but considerable attention must be paid to the convergence of the series. In this paper, $g(\tau)$ is obtained from a modified version of the integral representation of Pollard, by means of a 32-point Gauss–Laguerre quadrature

$$\begin{aligned}G(s) &= 1/\pi\int_0^\infty e^{-z}\{e^{-(zs)^\beta\cos\pi\beta} \\ &\quad \times \sin[(zs)^\beta \sin\pi\beta]\}\, dz\end{aligned} \tag{23}$$

where $g(\tau) = G(\tau)/\tau$ and $s = \tau/\tau_0$. Fig. 8 shows several DRT functions corresponding to WW response functions with $\beta = 0.1$, 0.3, 0.5 and 0.7.

In order to test the accuracy of the obtained WW parameters we have recalculated the $M^*(\omega)$ function from the previously estimated β and τ_0 values by means of the following relationship for $N^*(\omega)$ [30]

$$N^*(\omega) = \sum_{j=1}^{n} \frac{g_j}{1 + i\omega\tau_j} \tag{24}$$

which may be easily calculated by adopting a discrete representation for $\phi(t)$

$$\phi(t) = \sum_{i=1}^{n} g_i e^{-t/\tau_i} \tag{25}$$

where the coefficients g_i are a discretization of $g(\tau)$.

Once we have obtained the $N^*(\omega)$ function, the complex dielectric modulus is calculated according to Equation 13: the dots in Fig. 7 correspond to our recalculated $M^*(\omega)$ values which are in excellent agreement with the experimental ones.

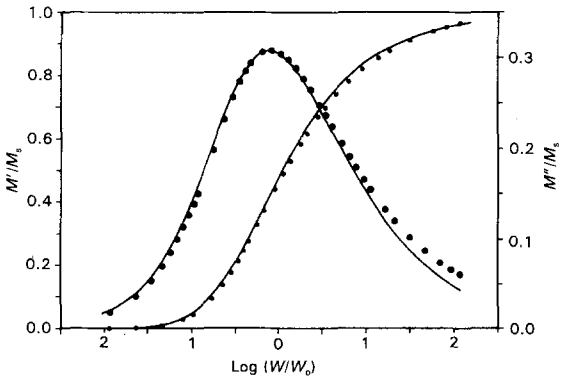

Figure 7 (———) Normalized real and imaginary parts of $M^*(\omega)$ versus the normalized frequencies $\omega_0 = 2\pi/\tau_0$ for a Y-FSZ sample at 503 K. (●, •) Reconstructed $M^*(\omega)$ response, via Equations 17 and 24, and illustrating the goodness of our β and $g(\tau)$ estimations. (●) M'/M_s, (•) M''/M_s.

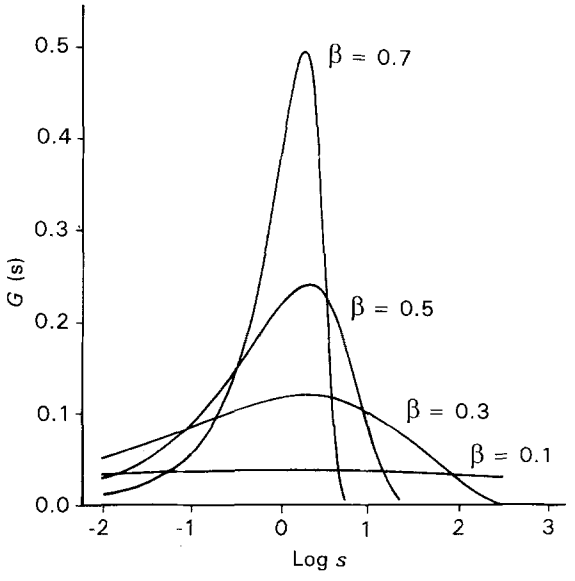

Figure 8 Distribution of relaxation times corresponding to the WW response for several values of β.

5. Estimation of g(τ) by successive approximations

As mentioned above, the $g(\tau)$ function corresponds to the inverse Laplace transform of the relaxation response function $\phi(t)$. Because $\phi(t)$ cannot be expressed such that a closed solution of $g(\tau)$ can be obtained, a number of approximate methods have been suggested [11, 33–35]. Recently, Agrawal and Zhang [11] have proposed the most simple method to approximate the $g(\tau)$ function, based on some relationships deduced by Schwarzl and Staverman [35]. In practice, they find that the DRT can be evaluated by

$$g_1(\ln\tau) = -|\mathrm{d}\phi/\mathrm{d}\ln t|_{t=\tau} \quad (26)$$

$$g_2(\ln\tau) = -|\mathrm{d}\phi/\mathrm{d}\ln t - \mathrm{d}^2\phi/\mathrm{d}(\ln t)^2|_{t=2\tau} \quad (27)$$

$$g_3(\ln\tau) = -|\mathrm{d}\phi/\mathrm{d}\ln t - 3/2\,\mathrm{d}^2\phi/\mathrm{d}(\ln t)^2 + 1/2\,\mathrm{d}^3\phi/\mathrm{d}(\ln t)^3|_{t=3\tau} \quad (28)$$

$$g_4(\ln\tau) = -|\mathrm{d}\phi/\mathrm{d}\ln t - 11/6\,\mathrm{d}^2\phi/\mathrm{d}(\ln t)^2 + \mathrm{d}^3\phi/\mathrm{d}(\ln t)^3 - 1/6\,\mathrm{d}^4\phi/\mathrm{d}(\ln t)^4|_{t=4\tau} \quad (29)$$

and so on, where $g_1(\ln\tau)$ is the first-order approximation and each higher approximation is closer to the true distribution: $g_\infty \equiv g(\tau)$. However, they do not evaluate the true $g(\tau)$ and limit themselves to generate, by an iterative process, successive distributions until the peak value of the next higher order did not vary from the preceding one by a certain percentage. It is evident that this method of exploring the validity of the proposed approximations strongly fails whenever the convergence rate is slow. Insofar as we can calculate the true $g(\tau)$ by the method outlined previously, we can perform a quick check on the order of approximation that would be required to generate a significant distribution function by this approximate method.

By adopting the WW dependence for $\phi(t)$ and applying the useful relation

$$\mathrm{d}\phi/\ln t = t\phi\,\mathrm{d}\ln\phi/\mathrm{d}t \quad (30)$$

the succesive differentiations of ϕ follows

$$\mathrm{d}\phi/\mathrm{d}\ln t = \beta\phi\ln\phi \quad (31)$$

$$\mathrm{d}^2\phi/\mathrm{d}(\ln t)^2 = \beta^2\phi\ln\phi(1+\ln\phi) \quad (32)$$

$$\mathrm{d}^3\phi/\mathrm{d}(\ln t)^3 = \beta^3\phi\ln\phi\{\ln\phi + (1+\ln\phi)^2\} \quad (33)$$

and so on. From these expressions the $g_n(\tau)$ approximations are readily evaluated.

Fig. 9 shows the true $g(\ln\tau)$ function (from $\beta = 0.2$–0.8) besides its successive approximations until the fourth-order versus normalized relaxation

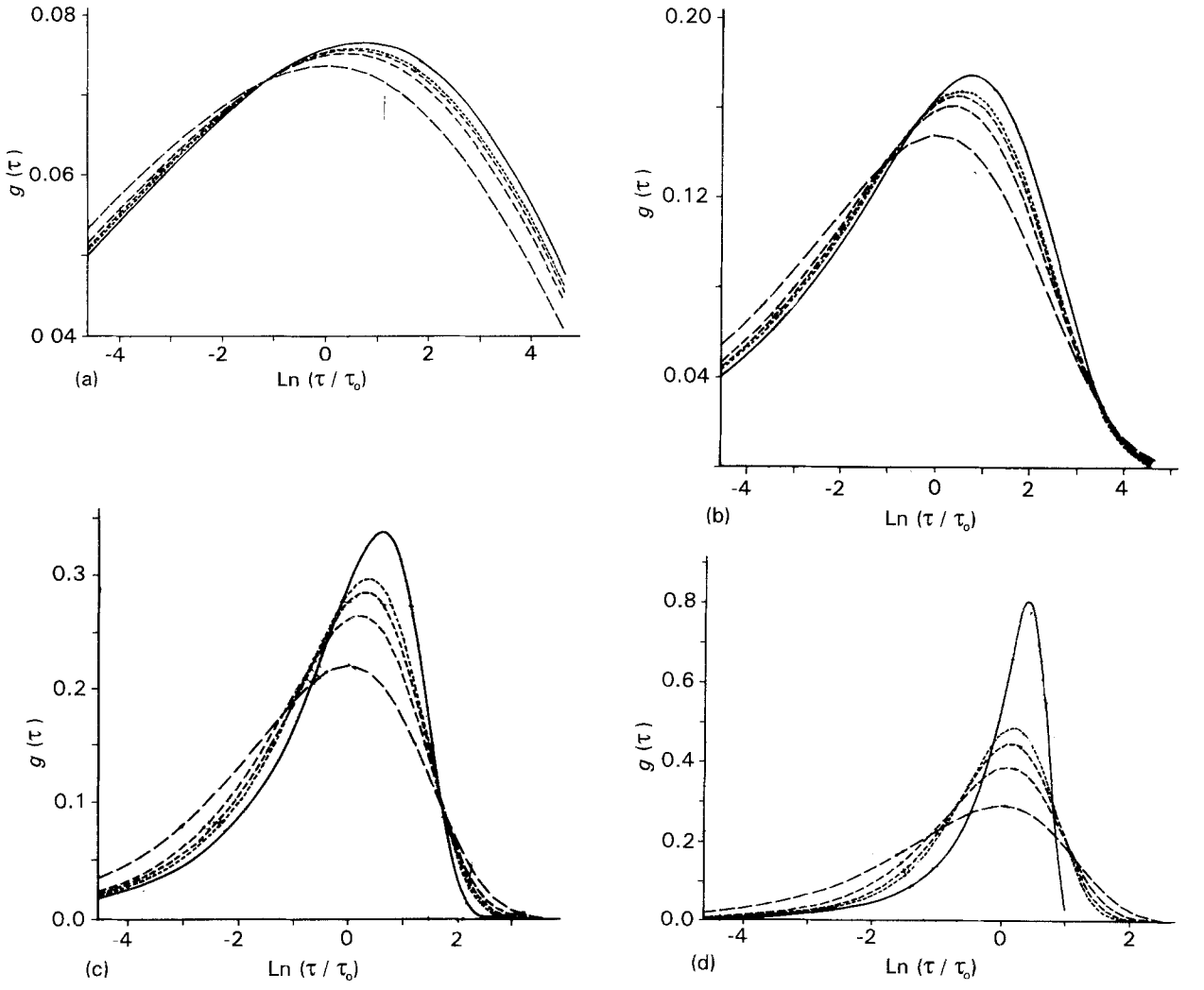

Figure 9 The first Agrawal four orders of approximation (dashed lines) and (———) the true $g(\ln\tau)$ distribution versus normalized relaxation times (τ/τ_0). (a) $\beta = 0.2$, (b) $\beta = 0.4$, (c) $\beta = 0.6$ and (d) $\beta = 0.8$. (— — — —) first order, (— — —) second order, (- - -) third order, (- - -) fourth order.

TABLE IV Goodness estimation of the successive approximation orders to the true $g(\tau)$ distribution. The estimation is based on d (the percentage of the differences between the first four orders and the true distribution)

	d (%)			
β	1st order	2nd order	3rd order	4th order
0.2	6.21	2.97	1.95	1.46
0.4	17.66	9.79	6.87	5.40
0.6	36.49	22.90	16.58	13.06
0.8	64.19	48.14	39.26	33.84

times, τ/τ_0 (τ_0 is the characteristic relaxation time of the WW dependence). A figure of merit (the percentage of the difference with respect to the true $g(\ln\tau)$) is evaluated in order to quantify the goodness of the respective approximations. The results are displayed in Table IV. It may be appreciated that the number of higher order approximations needed to produce the true spectrum depends on its sharpness and the quality of the approximation increases insofar as the shape of the distribution is wider. This observation agrees with Agrawal and Zhang's [11] result. In fact, $\beta = 0$ indicates an infinitely wide distribution while $\beta = 1$ corresponds to a single relaxation time. Our results indicate that this approximate method appears reliable whenever β is less than 0.2: in this case the first order of approximation yields a satisfactory estimate of $g(\ln\tau)$, and we disagree with the estimations of Agrawal and Zhang [11] about the order of approximation required to generate a significant distribution for each value of β. For example, Agrawal and Zhang have studied the volume relaxation of polystyrene with $\beta = 0.36$ and have found that a second-order of approximation suffices for a 5% error level. However, from Table IV it can be deduced that for this case, a fourth-order approximation is needed to reach the 5% error level. In practice, moreover, the observed values of β varies from 0.3–0.6 and for this reason we think that this approximate method which works well for very low values of β which do not occur in practice, is not satisfactory. For the other cases, the method demands higher orders of approximation, losing its simplicity and becoming non-competitive with the direct method to calculate the true $g(\ln\tau)$.

6. Activation energy spectra and the Williams–Watts response

Much past work associated with the structural relaxation in amorphous materials was based on the Gibbs *et al.* [36] activation energy spectrum (AES) model and with the pioneering Primak's work [12]. In the AES model, the change during relaxation at temperature, T, of a measured property, ΔP, is expressed by means of a Volterra integral equation of the first kind

$$\Delta P(t) = \int_0^\infty p_0(E)\theta(E, T, t)\,dE \qquad (34)$$

with kernel the characteristic annealing function, $\theta(E, T, t)$, and where $p_0(E)$ is the total property change in the energy range E to $E + dE$.

Following Primak [12], and assuming first-order reaction kinetics, the annealing function can be expressed as

$$\theta(E, T, t) = 1 - \exp[-\upsilon_0 t \exp(-E/kT)] \qquad (35)$$

υ_0 being an attempt frequency and k the Boltzmann constant. In fact, the functional form of $\theta(E, T, t)$ versus E, for given experimental values of T and t, is that of a sharp step at an energy $E_0 = kT \ln \upsilon_0 t$. Therefore, if we have to deal with broad and smooth AES we can replace the θ function by a step function: for $E \leq E_0$, the function has value of 1, and 0 for $E > E_0$. This approximation for $\theta(E, T, t)$ as a step function is equivalent to assuming that during an isothermal anneal, at time t, all processes with $E \leq E_0$ have contributed to the relaxation, whereas processes with $E > E_0$ have yet to contribute.

In the frame of this step-like approximation (the energy derivative method), one can easily prove that $p_0(E)$ is given by

$$p_0(E) = -\frac{1}{kT}\frac{d\Delta P}{d\ln t} \qquad (36)$$

In practice, according to the WW representation, we obtain the normalized spectrum

$$\Omega(E) = \frac{p_0(E)}{P_0 - P_\infty} = (\beta/kT)\,\phi(t)(t/\tau_0)^\beta \qquad (37)$$

The maximum of $\Omega(E)$, Ω_{max}, and its position, E_{max}, are given by

$$\Omega_{max} = e^{-1}\frac{\beta}{kT} \qquad (38)$$

$$E_{max} = kT(\ln \upsilon_0\tau_0 + \gamma) \qquad (39)$$

γ oeing the Euler's constant ($\gamma = 0.577, \ldots,$). It is sometimes suggested [37] that the temperature independence of the AES is a likely and plausible first assumption which stems from the "thermo-rheological simplicity principle". Consequently, the AES obtained from the same experiment but for different temperatures might superpose over a single AES. We have shown [37] that this requirement is equivalent to admitting a τ_0 thermally activated. This assumption allows us to obtain unambiguously the frequency factor, υ_0 [37].

Unfortunately, it is no longer possible in practice to support the drastic assumption about $\theta(E, T, t)$ and there is a need to develop a better and more general procedure of calculus: instead of calculating a continuous spectrum $p_0(E)$, we will calculate a discrete one: i.e. a discrete number of points p_{0j} at certain energies, E_j

$$p_{0j} = (1/\Delta E)\int_{E_j - \Delta E/2}^{E_j + \Delta E/2} p_0(E)\,dE \qquad (40)$$

By means of this step-wise approximation, the Volterra equation can be replaced by a set of linear equations which, in matrix notation, becomes

$$\boldsymbol{\Delta P} = \boldsymbol{A}\boldsymbol{p} \qquad (41)$$

where $\Delta \boldsymbol{P}$ and $\boldsymbol{p}$ are column matrix with n rows (n is the number of data points) and A is a nth order square matrix of the form

$$A_{i,j} = \int_{E_j - \Delta E/2}^{E_j + \Delta E/2} \theta(t_i, E)\, dE \tag{42}$$

Equation 41 has the solution

$$\boldsymbol{p} = A^{-1} \Delta \boldsymbol{P} \tag{43}$$

It turns out, however, that Equation 41 forms a so-called "ill conditioned" system resulting in very unstable solutions. In practice, resorting to the variational Cook's "least structure analysis [38, 39] allows us to get smooth and stable solutions. In this method, a structure function $S(\boldsymbol{p})$ is defined as a fourth difference operator satisfying our intuitive concepts of a structureless function. Thus, our purpose is to find the solution which minimizes $S(\boldsymbol{p})$ under the κ^2 constraint

$$\kappa^2 = \sum_{i=1}^{n} (\Delta P_{it} - \Delta P_{ie})^2 / \sigma_i^2 = n \tag{44}$$

ΔP_{it} and ΔP_{ie} being the calculated (via Equation 41) and the experimental (at time t_i) values of ΔP_i, respectively, and σ_i is its standard deviation.

Using methods of variational calculus, the following result is obtained

$$\boldsymbol{p} = [A + \lambda(\tilde{A})^{-1}(W)^{-1}S]^{-1} \Delta \boldsymbol{P} \tag{44}$$

where λ is a Lagrangian multiplier, W is a diagonal matrix with elements $W_{ii} = 1/\sigma_i^2$, $\tilde{A}$ is the transposed matrix A and S is the smoothing matrix associated to the $S(\boldsymbol{P})$ operator.

In order to asses the performance of the method, we consider two different experimental cases:

(i) a broad spectrum corresponding to the enthalpic relaxation of amorphous selenium around T_g. We have in this case $\beta = 0.41$;

(ii) the narrow and sharp spectrum obtained from mechanical stress relaxation experiments on CoO single crystals at 77 K. The choice of this case is related to the large value of β ($\beta = 0.83$) as it corresponds to the presence of only one operative mechanism: the Peierls mechanism.

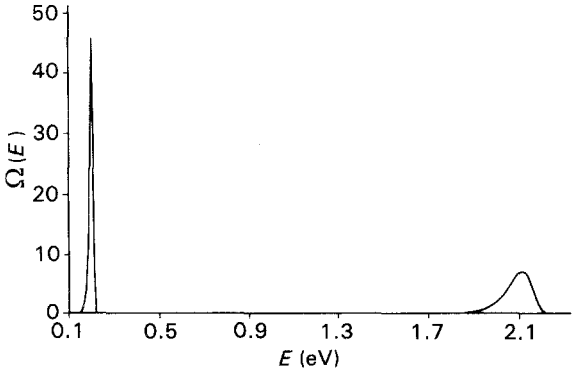

Figure 10 Comparison between the normalized approximate spectra describing the enthalpic relaxation of selenium (broad spectrum) and the stress relaxation CoO (sharp spectrum). Note the marked contrast between them.

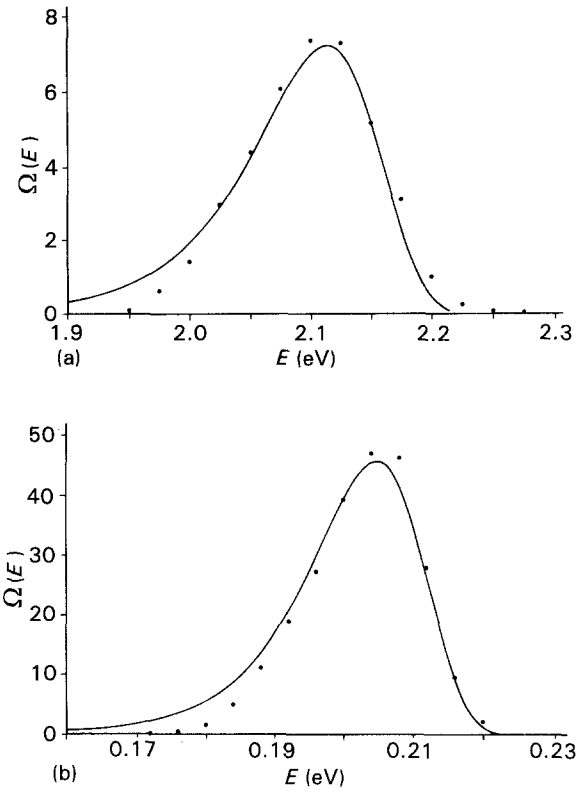

Figure 11 The approximate normalized spectra from Fig. 10 versus the "exact" discrete results derived by the method outlined in Section 6.

Fig. 10 shows, on the same scale, both AES which were calculated by the approximate method. Let us consider the maximum of the broad spectrum ($E \simeq 2.1$ eV at^{-1}): this result is in agreement with the Se–Se bond energy in trigonal-like chains and with the Perez interpretation [40, 41]. On the other hand, the maximum of the narrow spectrum is located at $E \simeq 0.2$ eV at^{-1}. This last value is intermediate between those associated with the Peierls stress for screw dislocations (0.15 eV at^{-1}) and that for edge dislocations (0.32 eV at^{-1}) [42].

Fig. 11 displays the approximate AES versus the exact ones. Both kinds of spectra are in fairly good agreement but the following comments may be made:

(i) the approximate spectra are skewed towards its low-energy side, while the "exact" ones are more symmetrical;

(ii) the reliability of the approximate AES appears to be inferior for the narrow spectrum. In fact, for this case, a slight shift between the maxima of both distributions may be appreciated.

Otherwise, the calculus complexity is by far superior for the new method and its application should be limited to the situations where it is called for. Thus, resort to the Primak's approximation appears widely justified if we are dealing with a broad and smooth spectrum and we are mainly interested in its general shape.

7. Conclusions

The main conclusion of this paper is that a large variety of relaxation phenomena for a wide class of

materials are well described by the WW function. It is worthwhile to remark that the response span covered by the different experiments analysed includes a broad interval of many decades in time for the characteristic relaxation times. Though the natural domain of the WW function is time, it has also been used with frequency domain data from dielectric–spectroscopy measurements. From this work, a connection between the relaxation function in the frequency domain and its corresponding WW transient response is established. On the other hand, miscellaneous topics related with the DRT or AES descriptions associated with the WW dependence have been discussed. The physical realisability of the obtained AES is supported by the simple and meaningful interpretation of the activation energies associated with its maxima. Then, in spite of some formal anomalies [10], we claim the utility of the WW representation. In fact, recent works [19, 43] show that the "universal" Havriliak–Negami frequency relaxation function (widely used to describe data from dielectric spectroscopies) fit closely the expected WW response. As pointed out by Alvarez *et al.* [19] the existence of simple empirical laws accounting for a variety of results, obtained by different probes over very different time-scales, strongly suggests that these relaxation phenomena should be projections of the same microscopic structural relaxation mechanisms.

References

1. K. S. COLE and R. H. COLE, *J. Chem. Phys.* **9** (1941) 341.
2. D. W. DAVIDSON and R. H. COLE, *ibid.* **19** (1951) 1484.
3. G. WILLIAMS and D. C. WATTS, *Trans. Faraday Soc.* **66** (1970) 80.
4. C. T. MOYNIHAN, L. P. BOESCH and N. L. LABERGE, *Phys. Chem. Glasses* **14** (1973) 122.
5. J. T. BENDLER and K. L NGAI, *Macromolecules* **17** (1984) 1174.
6. A. MUÑOZ and F. L. CUMBRERA, *Therm. Acta* **196** (1992) 137.
7. K. L. NGAI, A. K. RAJAGOPAL and C. Y. HUANG, *J. Appl. Phys.* **55** (1984) 15.
8. C. DE DOMINICIS, H. ORLAND and F. LAINEE, *J. Phys. Lett.* **46** (1985) L463.
9. E. W. MONTROLL and J. T. BENDLER, *J. Stat. Phs.* **34** (1984) 129.
10. J. R. MacDONALD, *J. Appl. Phys.* **62** (1987) R51.
11. A. AGRAWAL and R. L. ZHANG, *Phys. Chem. Glasses* **29** (1988) 141.
12. W. PRIMAK, *Phys. Rev.* **100** (1955) 1677.
13. J. CASTAING, M. SPENDEL, J.PHILIBERT, A. DOMINGUEZ-RODRIGUEZ and R. MARQUEZ, *Rev. Phys. Appl.* **15** (1980) 277.
14. F. GUIBERTEAU, M. JIMENEZ-MELENDO, A. DOMINGUEZ-RODRIGUEZ, R. MARQUEZ and J. CASTAING, *Cryst. Latt. Def. Amorph. Mater.* **16** (1987) 91.
15. A. MUÑOZ, F. L. CUMBRERA and R. MARQUEZ, "Current Topics on Non-Crystalline Solids" (World Scientific, Singapore 1986) p. 211.
16. F. L. CUMBRERA and A. MUÑOZ, *Therm. Acta* **144** (1989) 123.
17. R. B. STEPHENS, *J. Appl. Phys.* **49** (1978) 5855.
18. J. GRENET, J. P. LARMAGNAC, P. MICHON and C. VAUTIER, *Thin Solid Films* **76** (1981) 53.
19. F. ALVAREZ, A. ALEGRIA and J. COLMENERO, *Phys. Rev. B* **44** (1991) 7306.
20. D. W. MARQUARDT, *J. Soc. Ind. Appl. Math.* **11** (1963) 431.
21. J. C. LI, *J. Phys.* **45** (1967) 493.
22. D. J. LLOYD, P. J. WORTHINGTON and J. D. EMBURY, *Philos. Mag.* **22** (1970) 1147.
23. F. C. AIFANTIS and W. W. GERBERICH, *Mater. Sci. Eng.* **21** (1975) 107.
24. M. GROSBRAS, E. DEDIEU and M. CAHOREAU, *Phys. Status Solidi (a)* **42** (1977) 449.
25. G. SCHOECK, *ibid.* **87** (1985) 571.
26. K. K. RAY and A. K. MALLIK, *Mater. Sci. Eng.* **59** (1983) 59.
27. P. FELTHAM, J. Inst. Metals **89** (1961) 210.
28. A. G. EVANS and R. D. RAWLINGS, *Phys. Status Solids* **34** (1969) 9.
29. P. SARKAR and P. NICHOLSON, *J. Am. Ceram. Soc.* **72** (1989) 1447.
30. P. B. MACEDO, C. T. MOYNIHAN and R. BOSE, *Phys. Chem. Glasses* **13** (1972) 171.
31. J. D. FERRY, "Viscoelastic properties of Polymers" (Wiley, New York, 1961).
32. H. POLLARD, Bull. Am. Math. Soc. **52** (1946) 908.
33. J. D. FERRY and M. L. WILLIAMS, *J. Colloid. Sci.* **7** (1952) 347.
34. N. W. TSCHOEGL, "The theory of linear viscoelastic behaviour" (Academic Press, New York, 1981).
35. L. SCHWARZL and A. J. STAVERMAN, *Appl. Sci. Res.* **4** (1953) 127.
36. M. R. J. GIBBS, J. E. EVETTS and J. A. LEAKE, *J. Mater Sci.* **18** (1983) 278.
37. A. MUÑOZ, F. L. CUMBRERA and R. MARQUEZ, *Mater. Chem. Phys.* **21** (1989) 279.
38. B. C. COOK, *Nucl. Instrum. Meth.* **24** (1963) 256.
39. DE CEUNINCK, Z. RUYAN, G. KNUYT, L. SCHEPPER and L. M. STALS, *Mater. Sci. Eng.* **97** (1988) 545.
40. J. PEREZ, *J. de Phys.* **C10** (1985) 427.
41. *idem, Rev. Phys. Appl.* **21** (1986) 93.
42. A. DOMINGUEZ-RODRIGUEZ, J. CASTAING, H. KOISUMI and T. SUZUKI, *ibid.* **23** (1988) 1361.
43. J. COLMENERO, A, ALEGRIA, J. M. ALBERDI, F. ALVAREZ and B. FRICK, *Phys. Rev. B* **44** (1991) 7321.

Received 29 September 1992
and accepted 19 March 1993